DESIGN OF DISCRETE-TIME STATOR CURRENT CONTROLLER IN A HIGH PERFORMANCE AC DRIVE

\OR\E M. STOJI] AND SLOBODAN N. VUKOSAVI]

***Abstract* - This paper presents a novel ac motor current controller conceived for use on low-end μC. Simulation and experimental results show that are accomplished fast current response and robustness against the measurement noise and the drift in the parameter values. Simplicity and the ease of parameter setting in conjunction with a low μC throughput widen the field of possible applications. Proposed controller is, also, convenient because it doesn't require expensive sampling hardware and precise definition of the sampling point in the time.**

I. INTRODUCTION

Recent growth of ac drives application in industry has initialized development of discrete-time current controllers. Necessity of adopting full digital control is imposed by the required flexibility and compactness of digital control hardware. In industry and home appliances applications reliability and low price stand as the main requirements, and they can be easily achieved using full digital realizations.

The major problem of discrete current control is aliasing of high frequency noise during sampling. Presence of high frequency component in stator current is caused by the use of three phase PWM inverter as voltage actuator. Non-sinusoidal supply causes presence of current ripple, which has frequency close or even higher than the sampling frequency. In most realizations influence of current ripple is minimized using special sampling techniques that require hardware not included in the general purpose μC. Hence, development of simple method for current measurement appears as the main problem in design of controller.

Discrete current controller is created in order to enable implementation of the vector control algorithm on the ac motor. Since the torque of ac drive depends upon the stator current, good servo-actuator can be produced only if the good current regulation is provided. Value of steady-state error and response rise-time of the current determine characteristics of controller. Hence, the structure and parameters of controller are designed to provide zero error signal in steady-state and the bandwidth of control loop in the range 500 Hz - 1 kHz.

Variety of discrete-time current controllers is presented in the literature. The most frequently used solutions convey analog realizations. Expensive and unreliable hardware, together with problems of variable switching frequency and non-zero steady-state error, exclude analog regulators as the convenient solutions. Paper [1] presents analog hysteresis algorithm, emphasizing that the main difficulty of proposed solution is inadmissible large steady-state switching frequency, which generates large EMI and may cause IGBT thermal collapse. Fixed switching frequency is guaranteed in discrete controller realizations. Also, zero error signal in steady-state can be obtained with controller in synchronous frame. The most frequently used discrete controller conveys "dead-beat" algorithm, which provides minimum settling time of stator current response. In paper [3] is presented basic "dead-beat" discrete algorithm. In paper [4] is presented improved "dead-beat" algorithm with use the state variable observer, which enables estimation of the air-gap flux. Estimated flux value is used in the exclusion of EMS influence on the current wave form. Difficulties that occur in a realization of "dead-beat" controller are associated with very large ac motor line voltages that controller requires during the transient.

The problem of high frequency noise aliasing can be solved using one of following two solutions: (1) use of analog antialiasing filter and (2) application of special techniques which convey

sampling at the precise point in time when the value of stator current ripple equals zero. The use of antialiasing filter is discussed in paper [5]. There, second order Chebisev filter is proposed in order to eliminate influence of noise. Presented experimental results show that use of proposed analog filter deteriorates controller characteristics, which is the reason why antialiasing filter was not widely accepted as convenient solution. The use of special sampling techniques is presented in paper [6], which shows that the proposed method is erroneous in the case of ac motor with small stator resistance. Also, special sampling techniques require special measurement hardware outside μC, which is not acceptable from the point of compactness and low cost of control hardware.

The influence of time delay, introduced by control hardware, must be analyzed since duration of time lag is comparable with response time of current. Analysis of system dynamics in presence of time delay enables design of controller robust against influence of time lag. Such controller could be realized on slower and cheaper μC.

This paper suggest use of the first order antialiasing filter and the cascade controller in the synchronous frame. Proposed analog filter was used because it can eliminate noise components placed around sampling frequency multiples. These components alias into the Nyquist frequency band during sampling. Conversely to [6], sampling instance doesn't have to be precisely defined, which enables use of A/D converters included in μC. Simulation runs and experimental results show that is achieved system bandwidth larger than 500 Hz, for sampling period of 300 μs. Also, it is shown that the controller is robust against the drift of ac motor parameter values. Presented controller is realized using low cost 80196KB μC and the common measurement hardware.

Section II presents the structure of the discrete current controller. Section III presents the tuning procedure of controller parameters, together with simulation runs that confirm analytical considerations. Section IV presents experimental results measured on the developed ac drive. The summary and concluding remarks are given in Section V. Appendix I includes the transformation of the system model from stationary into the synchronous frame.

II. THE STRUCTURE OF SYNCHRONOUS REGULATOR WITH THE WEAK DEFINITION OF SAMPLING INSTANCE

Controller is designed in the synchronous frame. Since in the rotational frame all variables have direct values, it is possible to create controller which will guarantee the zero error signal in the steady-state. Samples of line currents i_a and i_b are transformed into variables i_q and i_d of the rotational frame, synchronous with the ac motor excitation vector. The sampling period is 300 μs. Line currents are sampled sequentially i_b after i_a, which introduces the weak definition of the sampling instance. The period of the sampling instance uncertainty is equal to the microcontroller's A/D conversion time $t_{A/D}$ = 20 μs.

Figure 1. presents the structure of the control system.

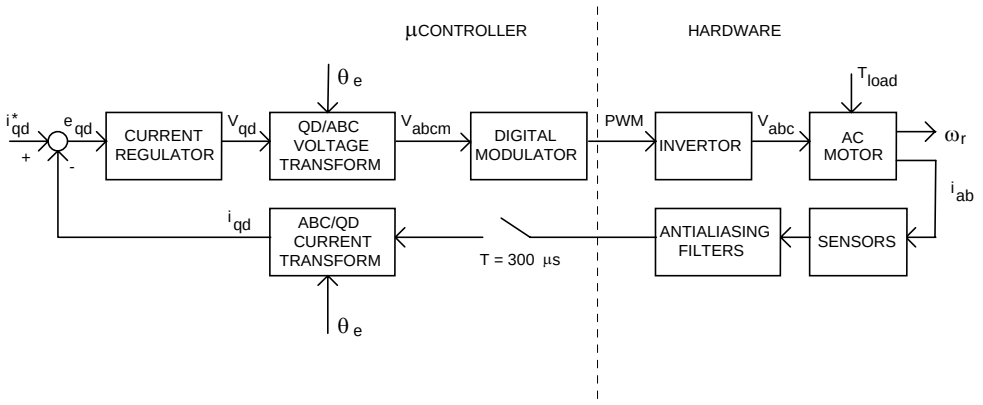

Figure 1. Block diagram of the control structure

At Fig.1 i_{qd}^* presents references for i_q and i_d, and θ_e presents angle of excitation vector. Current regulation is realized using two independent controllers, one for each of the currents i_q and i_d. Discrete transfer function of controller is given in the Eq. (1).

$$G_{con}(z) = K\,\frac{(z-\sigma)^2}{z(z-1)} \tag{1}$$

Controller references i_q^* and i_d^* are generated by the vector control algorithm. Values of variables i_q and i_d are obtained using the direct ab/qd transformation of filtered currents samples. The direct ab/qd transformation is carried out using following the Eq. (2).

$$\begin{bmatrix} i_q \\ i_d \end{bmatrix} = T \begin{bmatrix} i_a \\ i_b \end{bmatrix} = \begin{bmatrix} t_{11} & t_{12} \\ t_{21} & t_{22} \end{bmatrix} \begin{bmatrix} i_{af} \\ i_{bf} \end{bmatrix} = \frac{2}{\sqrt{3}} \begin{bmatrix} \sin\left(\omega_e t + \frac{\pi}{3}\right) & \sin(\omega_e t) \\ -\cos\left(\omega_e t + \frac{\pi}{3}\right) & -\cos(\omega_e t) \end{bmatrix} \begin{bmatrix} i_{af} \\ i_{bf} \end{bmatrix} \tag{2}$$

Command PWM signals for the three-phase inverter are generated using the digital modulator. Modulator inputs are line voltages's command signals V_{am}, V_{bm} and V_{cm}. These signals are obtained using the inverse qd/ab transformation of controller outputs V_q and V_q. The inverse qd/ab transformation is given in the Eq. (3).

$$\begin{bmatrix} V_{am} \\ V_{bm} \end{bmatrix} = T^{-1} \begin{bmatrix} V_q \\ V_d \end{bmatrix} = \begin{bmatrix} q_{11} & q_{12} \\ q_{21} & q_{22} \end{bmatrix} \begin{bmatrix} V_q \\ V_d \end{bmatrix} = \begin{bmatrix} \cos(\omega_e t) & \sin(\omega_e t) \\ -\cos\left(\omega_e t + \frac{\pi}{3}\right) & -\sin\left(\omega_e t + \frac{\pi}{3}\right) \end{bmatrix} \begin{bmatrix} V_q \\ V_d \end{bmatrix} \tag{3}$$

The third command signal V_{cm} is calculated from V_{cm} = - V_{am} - V_{bm}. The variable ω_e in equations (2) and (3) presents the angular speed of the excitation vector. The angle of the excitation vector is calculated from $\theta_e = \omega_e t$. Both θ_e and ω_e are generated by the vector control algorithm.

In the analysis of the control structure is necessary to define the model of ac motor stator circuit. The literature [2] contains the simplified model of the stator circuit. On Fig. 2 is given the model of one of the stator phases in the stationary frame.

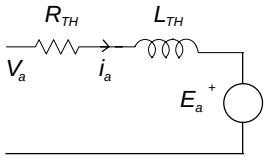

Figure 2. Used model of the ac motor stator model in the stationary frame

According to Fig. 2 we obtain following stationary frame model,

$$\begin{bmatrix} V_a \\ V_b \\ V_c \end{bmatrix} = R_{TH} \begin{bmatrix} i_a \\ i_b \\ i_c \end{bmatrix} + L_{TH} \frac{d}{dt} \begin{bmatrix} i_a \\ i_b \\ i_c \end{bmatrix} + \begin{bmatrix} E_a \\ E_b \\ E_c \end{bmatrix} \tag{4}$$

where E_a, E_b and E_c present induced stator EMS. According to [2] R_{TH} and L_{TH} present parameters of the equivalent Thevenin circuit of the ac motor stator. They are derived under the presumption that the ac motor magnetizing induction is large. They have values $R_{TH} = R_s + R_r$ and $L_{TH} = L_{ls} + L_{lr}$. Parameters R_r and R_s present rotor and stator resistances. Parameters L_{ls} and L_{lr} present stator and rotor leakage inductances.

This paper adopts the antialiasing filter in the stationary frame as the strategy of suppressing the current ripple. Used analog filter must comply with following three conditions: (1) the filter must have the unity gain, (2) the ripple of the sampled current mustn't exceed 0,5 % of the nominal ac motor current, and (3) at the frequency range of 0 Hz - 100 Hz filter mustn't introduce the phase lag larger

than 4° and the magnitude smaller than 0,99. Condition (2) is related to the attenuation of the filter at the sampling frequency. Condition (3) is important because the phase lag and the magnitude characteristics generated by the filter introduce the error in values of i_q and i_d current components.

The error that filter introduces in i_q and i_d values, caused by the phase lag and the amplitude attenuation, can be observed on the model of filter in the synchronous frame. Filtering of line currents i_a and i_b is carried out using two stationary frame filters, given in the Eq. (5).

$$\begin{bmatrix} \dot{x}_a \\ \dot{x}_b \end{bmatrix} = \left[\begin{array}{c|c} A_f & 0_{n\times n} \\ \hline 0_{n\times n} & A_f \end{array}\right] \begin{bmatrix} x_a \\ x_b \end{bmatrix} + \left[\begin{array}{c|c} B_f & 0_{n\times 1} \\ \hline 0_{n\times 1} & B_f \end{array}\right] \begin{bmatrix} i_a \\ i_b \end{bmatrix}$$
$$\begin{bmatrix} i_{af} \\ i_{bf} \end{bmatrix} = \left[\begin{array}{c|c} C_f & 0_{1\times n} \\ \hline 0_{1\times n} & C_f \end{array}\right] \begin{bmatrix} x_a \\ x_b \end{bmatrix} \tag{5}$$

According to the Appendix 1 model of filters in the rotational frame is given in the Eq. (6).

$$\begin{bmatrix} \dot{z}_q \\ \dot{z}_d \end{bmatrix} = \left[\begin{array}{c|c} A_f & -\omega_e \mathrm{I}_{n\times n} \\ \hline \omega_e \mathrm{I}_{n\times n} & A_f \end{array}\right] \begin{bmatrix} z_q \\ z_d \end{bmatrix} + \left[\begin{array}{c|c} B_f & 0_{n\times 1} \\ \hline 0_{n\times 1} & B_f \end{array}\right] \begin{bmatrix} i_q \\ i_d \end{bmatrix}$$
$$\begin{bmatrix} i_{qf} \\ i_{qf} \end{bmatrix} = \left[\begin{array}{c|c} C_f & 0_{1\times n} \\ \hline 0_{1\times n} & C_f \end{array}\right] \begin{bmatrix} z_q \\ z_d \end{bmatrix} \tag{6}$$

According to condition (1) used filters (5) have the unity gain. The static gain matrix of the system (6) can be derived according to [8]. The gain matrix contains direct and cross-coupling gains between input and filtered currents. Static gains are functions of the excitation angular speed ω_e, which introduces the steady-state error of i_{qf} and i_{df} comparing to i_q and i_d. The error of i_q and i_d causes the error of the excitation vector calculated by the vector control algorithm, which may degrade the ac drive characteristics. The error of the excitation vector is illustrated on the Fig. 3.

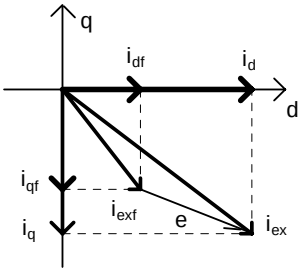

Figure 3. The error of the excitation vector caused by the antialiasing filters

The system magnitude from the line voltage input to the filter output, at the switching frequency ω_{sw}, is calculated from,

$$m_{v\_to\_c}(\omega_{sw}) = \frac{k_s \left|G_f(j\omega_{sw})\right|}{\sqrt{{\omega_{sw}}^2 L^2_{TH} + R^2_{TH}}} \cong \frac{k_s \left|G_f(j\omega_{sw})\right|}{(\omega_{sw} L_{TH})} \ . \tag{7}$$

In the Eq. (7) $G_f(j\omega)$ presents the frequency response of the filter. Also, k_s presents the gain of the current ripple introduced by uncertainty of the sampling instance. If uncertainty of the sampling instance would be equal to the half of PWM period we could measure the whole amplitude of the current ripple, and k_s would equal 1. Hence, we obtain k_s from $k_s = t_{un} / (T_s / 2)$. Since $t_{un} = t_{A/D} = 20$ μs and $T_s = 300$ μs, k_s equals $k_s = 0{,}134$. The illustration of k_s calculation is given on Fig. 4.

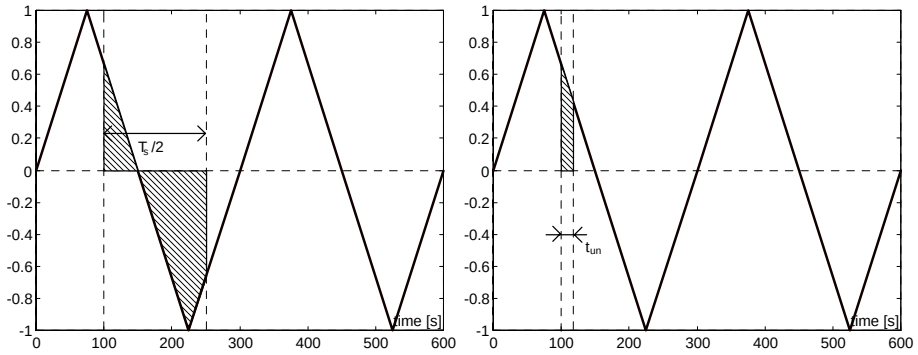

(a) (b)

Figure 4. Illustration of k_s calculation: (a) the worst case t_{un}= T_s / 2, and (b) t_{un}= $t_{A/D}$

For the nominal current of I_n = 10 A and the inverter DC-bus voltage of V_{DC} = 500 V, condition (2) is accomplished for the following value of magnitude,

$$m_{v\_to\_c}(\omega_{sw}) \le \frac{I_n}{200\ (V_{DC}/2)} = \frac{1}{5000}\ . \tag{8}$$

Using (7) and (8) for values of ω_{sw} = 20945 r/sec, L_{TH} = 0,023 H, and R_{TH} = 5,13 Ω, we obtain following condition,

$$\left|G_f(j\omega_{sw})\right| \le 0,72. \tag{9}$$

According to conditions (1), (3) and Eq. (9) we adopt following first order antialiasing filter,

$$G_f(s) = \frac{1}{\tau_f\ s+1} = \frac{1}{0.00005\ s+1}\ . \tag{10}$$

Function of the filter is not only to limit the sampled current ripple but, also, to suppress high frequency noise components from measurements. Experimental results in Section IV show that the proposed filter solves the problem of noise aliasing. For some systems the first order analog filter couldn't satisfy conditions (1), (2) and (3). In that case we propose the second order passive filters or the second order Chebisev active filters, presented in [5]. This problem could, also be solved with the use of the smaller sampling period.

III. THE CONTROLLER PARAMETER SETTING PROCEDURE

The controller is designed in order to achieve the bandwidth of the control loop larger than f_C = 500 Hz. The bandwidth of f_C = 500 Hz corresponds to the response rise time of i_{qf} and i_{df} equal to 800 μs [8]. The sampling time is determined as T_s < 1/2 f_C (= 0.001 sec). We adopt T_s = 0.0003 sec.

According to the Fig. 1 regulated plant is consisted of the digital modulator, inverter, ac motor, sensor, and the antialiasing filter. According to the Appendix 1 the plant model in the synchronous frame is given with the Eq. (11).

$$\begin{bmatrix}\dot{z}_1\\ \dot{z}_2\\ \dot{z}_3\\ \dot{z}_4\end{bmatrix}=\begin{bmatrix}-\frac{R_{TH}}{L_{TH}} & 0 & -\omega_e & 0\\ 1 & -\frac{1}{\tau_f} & 0 & -\omega_e\\ \omega_e & 0 & -\frac{R_{TH}}{L_{TH}} & 0\\ 0 & \omega_e & 1 & -\frac{1}{\tau_f}\end{bmatrix}\begin{bmatrix}z_1\\ z_2\\ z_3\\ z_4\end{bmatrix}+\begin{bmatrix}\frac{1}{\tau_f L_{TH}} & 0\\ 0 & 0\\ 0 & \frac{1}{\tau_f L_{TH}}\\ 0 & 0\end{bmatrix}\begin{bmatrix}V_q\\ V_d\end{bmatrix}+\begin{bmatrix}-\frac{1}{L_{TH}} & 0\\ 0 & 0\\ 0 & -\frac{1}{L_{TH}}\\ 0 & 0\end{bmatrix}\begin{bmatrix}E_q\\ E_d\end{bmatrix} \quad (11)$$

$$\begin{bmatrix}i_{qf}\\ i_{df}\end{bmatrix}=\begin{bmatrix}0 & k_m & 0 & 0\\ 0 & 0 & 0 & k_m\end{bmatrix}\begin{bmatrix}z_1\\ z_2\\ z_3\\ z_4\end{bmatrix}$$

In the Eq. (11) E_q and E_d are rotational transformations of stator EMS E_a, E_b, and E_c. Variables E_q and E_d have direct values, and they will be treated as external disturbances. In the Eq. (11) parameter k_m is given with $k_m = k_{mod}\, k_{A/D}$. The parameter k_{mod} presents the gain introduced by the digital modulator and the inverter (k_{mod} = 0,278). The parameter $k_{A/D}$ presents the gain introduced by the sensor and the A/D converter ($k_{A/D}$ = 51,2).

From the Eq. (11), using [8], we derive following set of analog pulse transfer functions.

$$\begin{bmatrix}i_{qf}(s)\\ i_{df}(s)\end{bmatrix}=\begin{bmatrix}G_p(s) & G_{cc}(s)\\ -G_{cc}(s) & G_p(s)\end{bmatrix}\begin{bmatrix}V_q(s)\\ V_d(s)\end{bmatrix} \quad (12)$$

Transfer functions $G_p(s)$ and $G_{cc}(s)$ vary with the change of ω_e . To simplify the controller design, the plant model for the excitation frequency $\omega_e = 0$ will be used. Experimental results will show if does exist the need for analysis of system dynamics for the case of $\omega_e > 0$. Reduced plant p.t.f, for $\omega_e = 0$, is given in the Eq. (13).

$$G_{rp}(s)=\frac{i_{qf}(s)}{V_q(s)}=\frac{i_{df}(s)}{V_d(s)}=\frac{k_m}{(L_{TH}s+R_{TH})(\tau_f s+1)} \quad (13)$$

To simplify the regulator synthesis, the pulse transfer function of system plant is calculated as the zero-hold equivalence of (13). Thus, according to [8], for parameter values of T = 300 μs, k_m = 14.23, R_{TH} = 5,14 Ω and $L_{\sigma S}$ = 0,023 H we obtain

$$G_{rp}(z)=\frac{i_{qf}(z)}{V_q(z)}=\frac{0.1504\ z+0.0287}{z^2-0.9378\ z+0.0023}. \quad (14)$$

Applied discretization method introduces error in the discrete model because the wave form of inverter output voltage was ignored. In [10], the more accurate p.t.f. of the system plant has been derived by the especial discretization technique. It takes into account the specific shape of ac motor input line voltage. However, only difference between the model developed in [10] and p.t.f. (14) consists in the position of real zero. For example, with the same parameter values, the p.t.f. developed in [10] has the zero at z = - 0.0481, while the zero of (14) is at z = - 0,1911. The difference becomes smaller as the sampling frequency increases. Nevertheless, for the sake of simplicity, we recommend the use of standard zero-hold equivalence decretization method. Namely, both simulation and experimental results show that error introduced by simplified discretization is negligible.

The discrete version of current control loop is shown in Fig. 3, where the transport lag z^{-1} is introduced to simulate the calculation of V_{qm}. In Fig. 5 $G_{con}(z)$ denotes the p.t.f. of used cascade controller, given in Eq. (1).

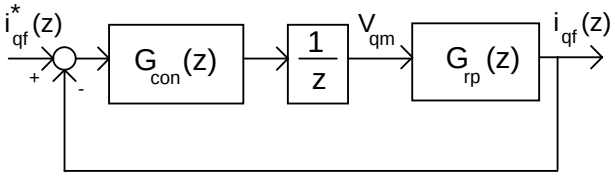

Figure 5. Discrete-time model of stator current control loop

The closed-loop transfer function of system in Fig. 5 is

$$G_s(z) = \frac{G_{con}(z)G_{rp}(z)}{z + G_{con}(z)G_{rp}(z)} \,. \tag{15}$$

Dominant poles $z_{1,2} = 0.2 \pm j\ 0.6$ of closed-loop p.t.f. (15) correspond to the required rise time of 800 μs, for the sampling period of $T = 0{,}0003$ s. Pole mapping of poles $z_{1,2}$ from Z-plane to S-plane gives equivalent dominant poles $s_{1,2} = -1527{,}2 \pm j\ 4163{,}5$. According to [8] system with dominant poles $s_{1,2}$ has rise time $t_{ri} \le 1/(-\mathrm{Re}(s_{1,2})) = 670$ μs, which satisfies condition of $t_{ri} \le 800$ μs. At the location of dominant poles $z_{1,2}$, the open-loop transfer function of uncompensated system

$$W(z) = \frac{G_{rp}(z)}{z} \tag{16}$$

has the angle

$$\varphi(z_{1,2}) = \angle W\ (z)\big|_{z\ =\ 0.2+j0.6} = -227^{\circ}. \tag{17}$$

According to the root locus method, the desired dominant closed-loop poles are obtained with the controller (1), which at the desired pole location has the angle

$$\varphi_{con} = \angle G_{con}\ (z)\big|_{z\ =\ 0.2+j0.6} = -180^{\circ} - \varphi(z_{1,2}) = 47^{\circ}. \tag{18}$$

Hence, the controller parameters are calculated from

$$\angle\left[K\frac{(z-\sigma)^2}{z\,(z-1)}\right]\Bigg|_{z\,=\,0.2+j0.6} = \varphi_{con} \tag{19}$$

to obtain

$$\sigma = 0.2 - 0.6\,\mathrm{ctg}\left(\frac{\varphi_{con} - 145^{\circ}}{2}\right) \tag{20}$$

and

$$K = \frac{|\,z\,|}{|\,G_{rp}(z)\ G_{con}(z)\,|}\Bigg|_{z\ =\ 0.2+j\ 0.6} \,. \tag{21}$$

The above equations yields $\sigma = 0.72$ and $K = 3.5$. Notice that outlined procedure of controller parameter setting may be applied in a general case. It should also be noticed that proposed regulator corresponds to the cascade PID controller given with equation (22)

$$G_{PID}\ (z) = K_p + K_i\ \frac{z}{z-1} + K_d\ \frac{z-1}{z} \tag{22}$$

for the parameter values of $K_p = 1.41$, $K_i = 0.27$, and $K_d = 1{,}82$.

Fig.6 shows the root locus of compensated system. The figure shows that the use of proposed cascade controller placed dominant poles into the desired locations. This control algorithm was tested

and verified for the widest possible range of ac drive model parameters that can be encountered in practice.

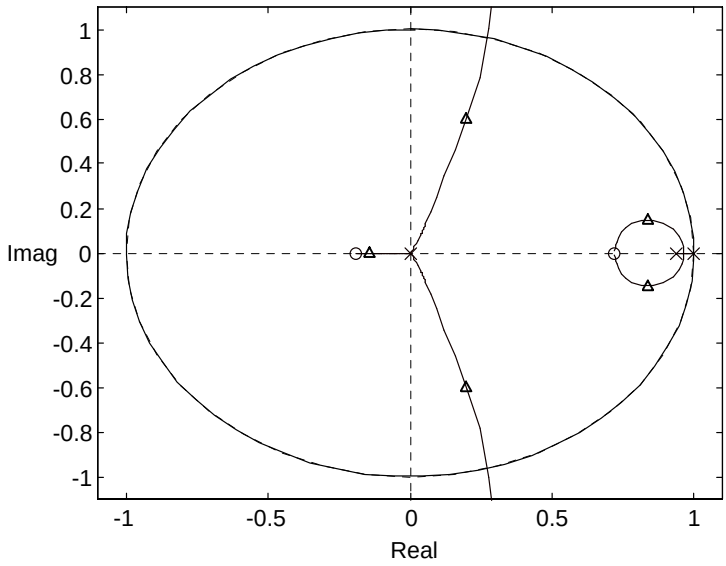

Figure 6. Root locus of compensated system

Robustness of controller will be examined using simulation results of system model, given on Fig.3. Simulation runs will be carried out for different values of R_{TH}, which corresponds to changes of rotor resistance. Influence of rotor resistance on R_{TH} is given with equation $R_{TH} = R_s + R_r$.

In Fig.7 are shown simulation runs for nominal values of stator parameters R_{TH} = 5,12 Ω and L_{TH} = 0,023 H.

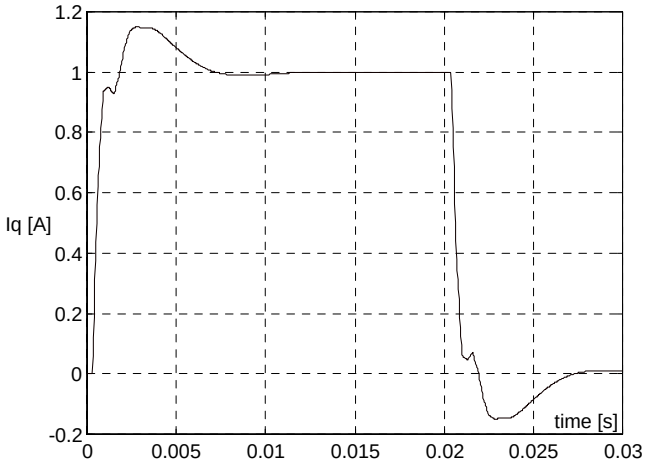

Figure 7. Current response for the nominal model values

Simulation traces in Fig.7 show that Iq stator current response matches the desired rise time less than t_{ri} = 800 μs. Also, Fig.7 shows that regulated current has reasonable overshot less than 20%.

Fig. 8 contains simulation runs for different values of R_{TH} . This should prove that controller is robust against changes of rotor resistance , which varies significantly during exploitation of ac drive.

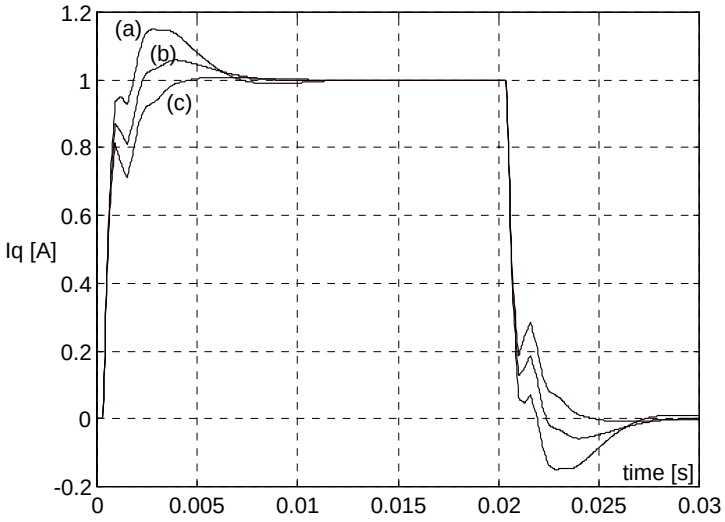

Figure 8. Iq stator current component step response for values of R_{TH} (a) 5.14 Ω, (b) 10 Ω, and (c) 15 Ω

Simulation runs from Fig.8 show that controller retains it's characteristics even for the drastic changes of rotor resistance.

IV. THE PRESENTATION OF EXPERIMENTAL RESULTS

The presented current regulator was realized using hardware setup based on 16-bit general purpose microcontroller INTEL 80196KB. Three-phase IGBT inventer, with nominal power of 10 kVA, was used as voltage actuator. Microcontroller's 10-bit resolution A/D converters were used of sampling of current signals. Three 16-bit counters were used for PWM signal generation. The algorithm was tested on the 6-pole asynchronous motor, with nominal power of 7.5 kW. The block diagram of hardware setup is shown at the Fig. 9.

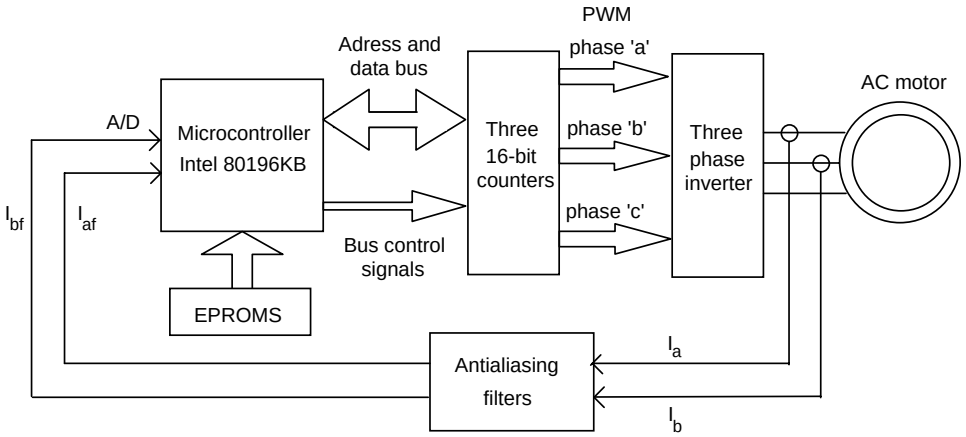

Figure 9. The control system hardware setup

In the Fig.10 are presented measurements of current I_q for excitation frequency of f_e = 34 Hz and fixed rotor shaft. The reference for I_q is I^*_q = 1 A. Traces in the Fig.10 are in agreement with related simulation results in the Fig.7. Notice that the speed of current response matches the desired value. Namely, the obtained rise time of t_{ri} = 600 μs is lower than maximum allowable value of 800 μ s. Because of the error introduced by qd-transformation appear fluctuations at the steady-state of I_q.

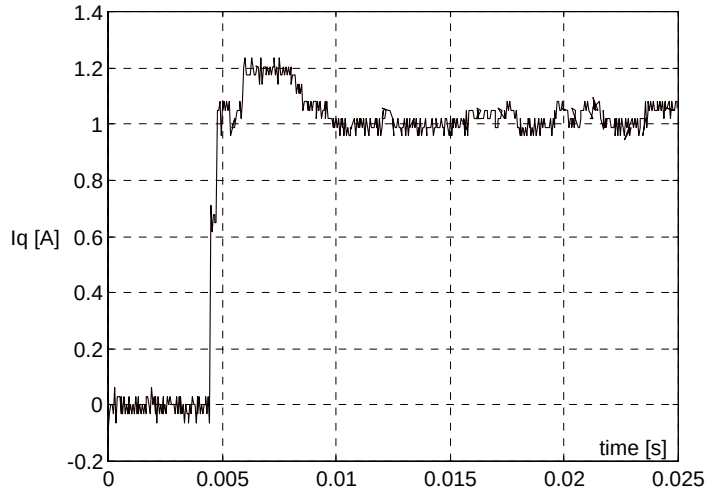

Figure 10. I_q current step response for I_q = 34 Hz and fixed rotor shaft

Fig. 11 shows the I_q current step response for the same excitation frequency and non zero speed of the motor shaft. This are the most representative results, since is in this case current regulation being carried out in presence of the external EMS disturbance. Fluctuations of I_q current are caused by the non-symmetry of the ac motor, which causes nonlinear distortion of the induced EMS. Never the less, current regulator eliminates influence of the external disturbance up to the point tolerable in high performance ac drive applications.

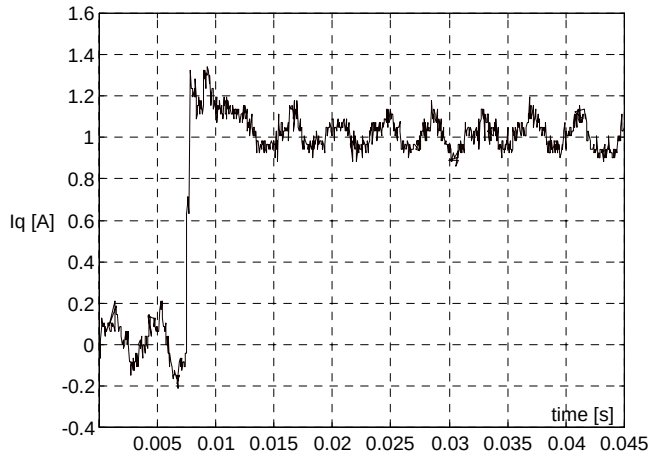

Figure 11. I_q current step response for I_q = 34 Hz and rotational rotor shaft

Results presented in the Fig. 11 prove that in the presence of external EMS disturbance regulator retains it's designed characteristics. Results from the Fig. 10 and the Fig. 11 show that the simplified plant model (13) can be successfully used instead of model (11).

The Fig. 12 contains steady-state stator current wave form for excitation frequency of 34 Hz and rotational rotor shaft, in order to prove that proposed control algorithm enables current regulation with very high clear factor of sinusoidal stator current.

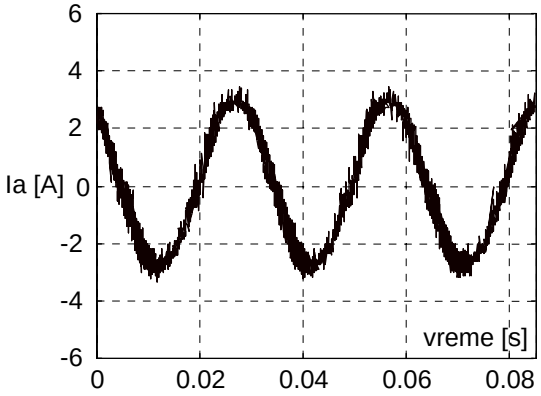

Figure 13. The steady-state line current for f_e= 34 Hz and rotational rotor shaft

V. THE CONCLUSION

This paper presents complete algorithm for synthesis of the current synchronous regulator. Controller structure was presented together with the effective parameter tuning algorithm, which enables fast and robust current control. Proposed controller was realized using the common measurement hardware and the general purpose microcontroller.

Presented control algorithm solves three problems that exist in the discrete current control. They are: current sampling in the presence of high frequency noise; the influence of time-delay introduced by control hardware; and realization of the fast current response. Also, this paper contains the complete parameter tuning method, which can be used for any set of ac motor parameters. Presented control structure can, also, be used in the variety of similar control problems. For example, it can be used in the control of DC motor currents or in the control of the direct rotor current of the synchronous machine.

The same hardware and software setup used for ac motor current control was upgraded with indirect vector control algorithm. The speed regulated ac drive was designed with the sampling period of T = 3 ms.

APPENDIX 1

Let's consider the three-phase symmetric system with the input vector $U = [u_a\ u_b\ u_c]^T$ and the output vector $Y = [y_a\ y_b\ y_c]^T$. For given variables are valid equations $u_a + u_b + u_c = 0$ and $y_a + y_b + y_c = 0$. The model of the system is given with the Eq. (23).

$$\begin{aligned} \dot{X}_{2n\times 1} &= \left[\begin{array}{c:c} A_{n\times n} & 0_{n\times n} \\ \hdashline 0_{n\times n} & A_{n\times n} \end{array}\right] X_{2n\times 1} + \left[\begin{array}{c:c} B_{n\times 1} & 0_{n\times 1} \\ \hdashline 0_{n\times 1} & B_{n\times 1} \end{array}\right] \begin{bmatrix} u_a \\ u_b \end{bmatrix} \\ \begin{bmatrix} y_a \\ y_b \end{bmatrix} &= \left[\begin{array}{c:c} C_{1\times n} & 0_{1\times n} \\ \hdashline 0_{1\times n} & C_{1\times n} \end{array}\right] X_{2n\times 1} \end{aligned} \tag{23}$$

It is necessary to carry out the ab/qd rotational transformation of the three-phase system variables. The transformation of variables is done using equations

$$\begin{bmatrix} u_q \\ u_d \end{bmatrix} = T \begin{bmatrix} u_a \\ u_b \end{bmatrix}, \begin{bmatrix} y_q \\ y_d \end{bmatrix} = T \begin{bmatrix} y_a \\ y_b \end{bmatrix}. \tag{24}$$

The transformation matrix T is given in Eq. (2). From (24) we derive the inverse qd/ab transformation given with following equations

$$\begin{bmatrix} u_a \\ u_b \end{bmatrix} = T^{-1} \begin{bmatrix} u_q \\ u_d \end{bmatrix}, \begin{bmatrix} y_a \\ y_b \end{bmatrix} = T^{-1} \begin{bmatrix} y_q \\ y_d \end{bmatrix}. \tag{25}$$

The inverse transformation matrix T^{-1} is given with the Eq. (3).

To obtain the model of (23) in the synchronous qd frame it is necessary to perform the rotational transformation of the state variables vector *X*. According to (23) and (24) we derive

$$\begin{bmatrix} y_q \\ y_d \end{bmatrix} = T \begin{bmatrix} y_a \\ y_b \end{bmatrix} = T \left[\begin{array}{c:c} C_{1\times n} & 0_{1\times n} \\ \hdashline 0_{1\times n} & C_{1\times n} \end{array}\right] X_{2n\times 1} = \left[\begin{array}{c:c} C_{1\times n} & 0_{1\times n} \\ \hdashline 0_{1\times n} & C_{1\times n} \end{array}\right] Z_{2n\times 1}. \tag{26}$$

The transformation of state variables is carried out using following equation

$$Z = P\,X,\ P = \left[\begin{array}{c:c} t_{11}\,\mathrm{I}_{n\times n} & t_{12}\,\mathrm{I}_{n\times n} \\ \hdashline t_{21}\,\mathrm{I}_{n\times n} & t_{22}\,\mathrm{I}_{n\times n} \end{array}\right] = \frac{2}{\sqrt{3}} \left[\begin{array}{c:c} \sin\left(\omega_e t + \frac{\pi}{3}\right)\mathrm{I}_{n\times n} & \sin(\omega_e t)\,\mathrm{I}_{n\times n} \\ \hdashline -\cos\left(\omega_e t + \frac{\pi}{3}\right)\mathrm{I}_{n\times n} & -\cos(\omega_e t)\,\mathrm{I}_{n\times n} \end{array}\right]. \tag{27}$$

The inverse state variables transformation is done using the Eq. (28).

$$X = P^{-1}\,Z,\ P^{-1} = \left[\begin{array}{c:c} q_{11}\,\mathrm{I}_{n\times n} & q_{12}\,\mathrm{I}_{n\times n} \\ \hdashline q_{21}\,\mathrm{I}_{n\times n} & q_{22}\,\mathrm{I}_{n\times n} \end{array}\right] = \left[\begin{array}{c:c} \cos(\omega_e t)\,\mathrm{I}_{n\times n} & \sin(\omega_e t)\,\mathrm{I}_{n\times n} \\ \hdashline -\cos\left(\omega_e t + \frac{\pi}{3}\right)\mathrm{I}_{n\times n} & -\cos\left(\omega_e t + \frac{\pi}{3}\right)\mathrm{I}_{n\times n} \end{array}\right] \tag{28}$$

Elements t_{ij} of the matrix *P* are given in the Eq. (2). Elements q_{ij} of the matrix P^{-1} are given in the Eq. (3). Also, we shell need the following matrix *D*

$$D_{2\times 2} = \frac{d}{dt}\left(T^{-1}\right) = \begin{bmatrix} d_{11} & d_{12} \\ d_{21} & d_{22} \end{bmatrix} = \begin{bmatrix} -\omega_e \sin(\omega_e t) & \omega_e \cos(\omega_e t) \\ \omega_e \sin\left(\omega_e t + \frac{\pi}{3}\right) & -\omega_e \cos\left(\omega_e t + \frac{\pi}{3}\right) \end{bmatrix} \tag{29}$$

in order to derive the matrix *V*, given in the Eq. (30).

$$V = \frac{d}{dt}\left(P^{-1}\right) = \left[\begin{array}{c:c} d_{11}\,\mathrm{I}_{n\times n} & d_{12}\,\mathrm{I}_{n\times n} \\ \hdashline d_{21}\,\mathrm{I}_{n\times n} & d_{22}\,\mathrm{I}_{n\times n} \end{array}\right] = \left[\begin{array}{c:c} -\omega_e \sin(\omega_e t)\,\mathrm{I}_{n\times n} & \omega_e \cos(\omega_e t)\,\mathrm{I}_{n\times n} \\ \hdashline \omega_e \sin\left(\omega_e t + \frac{\pi}{3}\right)\mathrm{I}_{n\times n} & -\omega_e \cos\left(\omega_e t + \frac{\pi}{3}\right)\mathrm{I}_{n\times n} \end{array}\right] \tag{30}$$

In the Eqs. (29) and (30) ω_e presents angular speed of the rotational qd frame. According to (25) and (28) we obtain from (23) following differential equation,

$$\frac{d}{dt}\left(P^{-1}Z\right) = \left[\begin{array}{c:c} A & 0_{n\times n} \\ \hdashline 0_{n\times n} & A \end{array}\right]\left(P^{-1}Z\right) + \left[\begin{array}{c:c} B & 0_{n\times 1} \\ \hdashline 0_{n\times 1} & B \end{array}\right] T^{-1} \begin{bmatrix} u_q \\ u_d \end{bmatrix}. \tag{31}$$

The Eq. (31) is derived in the following manner.

$$\frac{d}{dt}\left(P^{-1}\right)Z + P^{-1}\dot{Z} = \left[\begin{array}{c:c} A & 0_{n\times n} \\ \hdashline 0_{n\times n} & A \end{array}\right]\left(P^{-1}Z\right) + \left[\begin{array}{c:c} B & 0_{n\times 1} \\ \hdashline 0_{n\times 1} & B \end{array}\right] T^{-1} \begin{bmatrix} u_q \\ u_d \end{bmatrix} \tag{32}$$

According to Eq. (30) we obtain

$$P^{-1}\dot{Z} = \left(\left[\begin{array}{c:c} A & 0_{n\times n} \\ \hdashline 0_{n\times n} & A \end{array}\right] P^{-1} - V\right) Z + \left[\begin{array}{c:c} B & 0_{n\times 1} \\ \hdashline 0_{n\times 1} & B \end{array}\right] T^{-1} \begin{bmatrix} u_q \\ u_d \end{bmatrix}. \tag{33}$$

From the Eq. (33) we obtain

$$\dot{Z} = \left(P \left[\begin{array}{c:c} A & 0_{n\times n} \\ \hdashline 0_{n\times n} & A \end{array}\right] P^{-1} - P\,V\right) Z + P \left[\begin{array}{c:c} B & 0_{n\times 1} \\ \hdashline 0_{n\times 1} & B \end{array}\right] T^{-1} \begin{bmatrix} u_q \\ u_d \end{bmatrix}. \tag{34}$$

Substituting (3), (27), (28), and (30) into the Eq. (34) we obtain

$$\dot{Z} = \left[\begin{array}{c:c} A & -\omega_e\,\mathrm{I}_{n\times n} \\ \hdashline \omega_e\,\mathrm{I}_{n\times n} & A \end{array}\right] Z + \left[\begin{array}{c:c} B & 0_{n\times 1} \\ \hdashline 0_{n\times 1} & B \end{array}\right] \begin{bmatrix} u_q \\ u_d \end{bmatrix}. \tag{35}$$

From the Eq. (26) we have

$$\begin{bmatrix} y_q \\ y_d \end{bmatrix} = \left[\begin{array}{c:c} C & 0_{1\times n} \\ \hdashline 0_{1\times n} & C \end{array}\right] Z \,. \tag{36}$$

The equations (35) and (36) present the model of the system (23) in rotational qd frame with the rotational angular speed of ω_e.

REFERENCES

[1] A. Tripathi and P. C. Sen, "Comparative analysis of fixed and sinusoidal band hysteresis current controllers for voltage source inverters", *IEEE Trans. on Industrial Electronics*, vol. 3, N№ 1, Feb. 1992, pp. 63-73.

[2] B. K. Bose, *Power electronics and ac drives*, Prentice-Hall, New Jersey, 1986.

[3] D. S. Oh, K. Y. Cho and M. J. Youn, "A discretized current control technique with delayed input voltage feedback for a voltage-fed PWM inverter", *IEEE Trans. on Power Electronics*, vol. 7, N№ 2, April 1992, pp. 364-373.

[4] L. Ben-Brahim, A. Kawamura, "Digital control of induction motor current with deadbeat response using predictive state observer", *IEEE Trans. on Power Electronics*, vol. 7, N№ 3, July 1992, pp. 551-559.

[5] R. B. Sepe, J. H. Lang, "Implementation of discrete-time field oriented current control", *IEEE Trans. on Industry Applications*, , vol 30, N№ 3, May/June 1994. pp. 723-728.

[6] G. Pfaff, A. Weschta, and A. Wick, "Design and experimental results of a brushless ac servo drive" in *Conf. Rec. IEEE Ind. Applicat. Soc. Annu. Meeting*, San Francisco, CA, 1982, pp. 692-697.

[7] Paul C. Krause, *Analysis of Electric Machinery*, McGraw-Hill Book C№· , New York, 1986.

[8] M. R. Stoji}, *Digital Control Systems*, Science, Belgrade, 1994 (Third edition, in Serbian).

[9] \.M. Stoji}, "Design of digital current controller in ac drives," *M.Sc. Thesis*, University of Belgrade, Faculty of Electrical Engineering, Belgrade, 1996.